THE ASTROPHYSICAL JOURNAL, 295:402–421, 1985 August 15

MOLECULAR GAS AT HIGH GALACTIC LATITUDES

LORIS MAGNANI AND LEO BLITZ[1]
Astronomy Program, University of Maryland

AND

LEE MUNDY
Astronomy Department, University of Texas
Received 1984 November 6; accepted 1985 February 22

ABSTRACT

This paper presents quantitative results of a CO survey of high-latitude molecular gas, the partial results of which were reported by Blitz, Magnani, and Mundy. We have found 57 clouds in 35 complexes at $|b| \geq 25°$. Maps of 33 of the clouds are presented, as are ^{13}CO and CO($J = 2$–1) observations. Seventy percent of the clouds are associated with optical emission. The clouds are shown to be distributed asymmetrically with respect to $b = 0°$; the distribution is consistent with a displacement of the Sun of 30 pc above the midplane. A gap in the cloud distribution in the northern Galactic hemisphere from $180° < l < 340°$ mimics that found in H I. Individual clouds subtend areas from a fraction of a square degree to several square degrees. Several of the mapped clouds are filamentary in shape, including a complex which extends perpendicular to the plane nearly 10°. At least one of the clouds has formed a T Tauri star, and three others show nebulosity which may be related to sites of star formation. Since the mean distance to the clouds is ~ 100 pc, the clouds are the nearest molecular clouds to the Sun and may contain the nearest regions of star formation. Quantities such as the mass, size, density, extinction, internal velocity dispersion, and $N(H_2)/N$(H I) are reported and found to be consistent with values presented previously. Notable among the nondetections are *IRAS* high-latitude "cirrus" clouds A, B, C, D, and X reported by Low *et al.*

Subject headings: galaxies: Milky Way — galaxies: structure — interstellar: molecules — stars: formation

I. INTRODUCTION

During the past decade, surveys of the molecular content of the Milky Way have been undertaken by many groups (Stark 1979; Burton and Gordon 1978; Blitz, Fich, and Stark 1982; Robinson *et al.* 1983; Israel *et al.* 1984; Dame 1984; Sanders, Solomon, and Scoville 1984). Because these surveys have been of material closely confined to the Galactic plane, very little is known about the molecular gas very close to the Sun which should occur predominantly at high galactic latitudes. Although a few isolated objects such as L134 and L1642 have been observed at high Galactic latitudes, there was no systematic search for molecular material at $|b| > 20°$ prior to the survey reported in Blitz, Magnani, and Mundy (1984, hereafter Paper I).

Paper I presented a summary of the initial survey of regions of apparent high-latitude extinction and reported the detection of a large number of molecular clouds. Subsequently, the survey has been extended and most of the detected objects have been mapped. This paper presents the results of the extended survey, including a catalog and maps of the clouds which could not be included in Paper I.

In § II of this paper we elaborate on the selection criteria and the data acquisition for the survey. In § III we examine the distribution of the sources as well as the observed properties of the clouds (morphology, temperatures, velocity structure, velocity dispersions, and isotope ratios). The correlation of molecular material with H I is discussed, as is the possibility of star formation in the high-latitude clouds. In § IV we use the observed properties obtained in § III to determine quantities such as mean distance, size, column density, mass, and extinction. The gravitational stability of the objects is examined and the total number and surface density are calculated. In § V the conclusions of the paper are presented.

II. OBSERVATIONAL PROCEDURE

a) Selection of Objects

Candidate regions for the "search" catalog were determined by looking for apparent optical obscuration on the Palomar Observatory Sky Survey (POSS) prints and the Whiteoak extension to the POSS. The search was limited to latitudes greater than $|b| = 20°$ and declinations greater than $\delta = -44°$. The choice $|b| \geq 20°$ was made because at these latitudes there did not appear to be any evidence for molecular material connected to lower latitude molecular gas. Each red and blue print was examined for regions greater than 5′ in diameter which showed: (1) a noticeable drop in star density, (2) any emission with a sharp boundary, possibly indicating the edge of a dark cloud, or (3) any change in the stellar density from the blue to the red print possibly indicating reddening due to dust. At latitudes 60° or greater, candidate regions become especially difficult to identify because of the paucity of stars and the relatively large stellar density fluctuations. The lack of blue prints for the Whiteoak extension complicated the search in the range $-44° < \delta < -37°$.

In many instances, candidate regions extend over a large area of the plate, or several regions occur in close proximity; several points with these areas were therefore listed. The search catalog was made without consulting the existing catalogs of high-latitude extinction. Nevertheless, the few previously cataloged objects at $|b| \geq 20°$ such as the Lynds (1962) dark clouds, or the regions associated with CO emission found near Sharpless (1959) H II regions (Blitz, Fich, and Stark 1982), were

[1] Alfred P. Sloan Foundation Fellow.

independently found in our perusal of the prints. The majority of objects in our search catalog are new; it is a list of any area at high latitude which appears to contain obscuring matter and perhaps molecular material.

The initial list contained 458 candidate regions but was not expected to be complete because of the subjective nature of the criteria used in selecting the candidate areas. After our first observing run, it became clear that many of our detections were associated with bright optical nebulosity on the POSS. Looking at the POSS plates again for high-latitude optical *emission*, we subsequently identified 35 additional regions of apparent obscuration. Many of the bright areas have been noted by Sharpless (1959) and Lynds (1965).

b) Observations

The observations were carried out using the 5 m telescope (HPBW = 2:3 at 115 GHz) of the Millimeter Wave Observatory[2] (MWO) near Fort Davis, Texas, at various times from 1983 November through 1984 June. The initial observations and maps were all made in in the CO(J = 1–0) transition at 115.2712 GHz. The receiver employed on the runs uses a helium-cooled Schottky-barrier diode mixer and has a single sideband (SSB) noise temperature of 220 K. Typical SSB system temperatures referred outside the atmosphere were 550–1000 K during the November and December runs and 650–1300 K during the May/June run. The initial observations were frequency-switched generally by 4 MHz and the typical rms noise with 5 minute integrations was 0.20 K. The telluric CO line was seen in every spectrum during the November and December runs and occasionally occurred at the same velocity as a source detection. Positions where the telluric line blended with emission from a source were reobserved in the position-switching mode, as were all weak signals. During the 1984 May/June run, the telluric line was weaker by a factor of 4 compared to the November and December observations, making it difficult to detect in an individual scan. This indicates a possible seasonal variation in the CO content of the upper atmosphere. The mapping was generally done in a frequency-switched mode with 2 minute integrations.

Signals were simultaneously processed using filter banks with 250 kHz and 62.5 kHz filters, which provided a resolution of 0.65 and 0.17 km s^{-1} respectively. The spectrometer was always centered at a velocity of 0.0 km s^{-1} relative to the local standard of rest (LSR) during the survey, and the velocity coverage was $\pm$89.5 km s^{-1} in the 250 kHz filters and $\pm$23.4 km s^{-1} in the 62.5 kHz filters, so that most of the sources appeared in both filter banks.

Calibrations using an ambient temperature chopper wheel (Penzias and Burrus 1973) were performed before observing any new source, and standard sources, such as Orion KL and the Rosette molecular cloud source A1-1 (Blitz and Thaddeus 1980), were observed periodically. The total variation in these standard sources was less than 5% during the runs. We present our results as T_A^*, the antenna temperature corrected for atmospheric attenuation, ohmic losses, and rearward spillover (Kutner and Ulich 1981). In order to compute $N(H_2)$ using LTE assumptions (see § IV*b*), it is necessary to determine the source radiation temperature T_R, which is given by $T_R = T_A^*/\eta_{FSS}\eta_c$, where η_c is the efficiency of the antenna coupling to the source and η_{FSS} is the forward hemisphere spillover and scattering coupling efficiency. At 115 MHz, the source coupling efficiency ($\eta_{FSS}\eta_c$) is 0.8 for sources larger than 30′ in diameter (Mundy, private communication). We use this value for all our calculations involving T_R.

Additional, less extensive observations were carried out at various other times: In 1983 December the ^{13}CO(J = 1–0) line at 110.2014 GHz was observed along 17 lines of sight. The standard ^{13}CO(J = 1–0) line strengths for Orion A and NGC 2024 are $T_A^* = 11.6$ K and $T_A^* = 22.1$ K respectively. At MWO, however, we obtained values of 8.6 K and 16.4 K for reasons that are unclear as of this writing. Therefore, for calculations of the molecular column densities (see § IV*b*) the ^{13}CO antenna temperatures are scaled upward by a factor of 1.35. This correction factor is not applied to the antenna temperatures in Table 4. The uncertainty in this factor for each source is about 15% (Mundy, private communication). For integrations of 15 to 30 minutes, the rms noise ranged from 0.03 K to 0.1 K. Observations of the CO(J = 2–1) line at 230.5380 GHz were made toward eight of our sources along 14 lines of sight during 1984 January, and the ^{13}CO(J = 2–1) line at 220.3987 GHz was observed in one of our objects during 1984 February. In 1984 February, cloud 57 was detected in the CO(J = 2–1) line, although we have not observed it in the CO(J = 1–0) transition.

III. RESULTS

a) Detections

Of the 493 candidate regions in the catalog, 488 were observed (5 could not be reached by the telescope because of pointing limits near the north celestial pole), and CO was detected from 133 positions. The results of the observations are presented in Tables 1 and 2, where the former lists objects at latitude $25° > |b| \geq 20°$, and the latter lists objects with $|b| \geq 25°$. Our results are divided into two latitude regions because the region with $|b| < 25°$ appears to include the northernmost or southernmost extensions of known molecular complexes at lower latitudes (such as the ρ Oph complex); thus it is not clear whether the clouds in this region are part of the high-latitude ensemble. In Table 1, the first column denotes the object number, the second through fifth list the α(1950), δ(1950), l, and b of the object. Object numbers 1–100 are reserved for clouds with $|b| \geq 25°$, and object numbers above 100 are for clouds with $20° \leq |b| < 25°$. The position for the clouds in Table 1 corresponds to the one in our original search catalog and does not necessarily reflect the central or strongest emission position of the source. The sixth, seventh, and eighth columns give T_A^*, the velocity with respect to the LSR in km s^{-1}, and the FWHM in km s^{-1} for the CO(J = 1–0).

The detections at $|b| \geq 25°$ are divided into 34 kinematically distinct complexes based on proximity in the sky and similarity of radial velocities. An additional complex was detected in the CO(J = 2–1) line for a total of 35 complexes at $|b| \geq 25°$. Many of the regions which were mapped show from two to four individual clouds separated by 10′–50′. Each spatially isolated cloud or cloudlet (as determined by an antenna temperature contour of 0.5 K) is considered a separate entity and is numbered accordingly.

In Table 2, the first column denotes the number of a complex and the second column denotes the individual cloud number. The third through sixth columns give the position of the individual clouds. The position corresponds to the strongest integ-

[2] The Millimeter Wave Observatory is operated by the Electrical Engineering Research Laboratory of the University of Texas at Austin with support from the National Science Foundation and McDonald Observatory.

TABLE 1

Clouds $20^\circ < |b| < 25^\circ$
[CO($J = 1$–0)]

Cloud	α (1950)	δ (1950)	ℓ	b	T_A^* (K)	V_{LSR} (km s^{-1})	Δv (km s^{-1})	Comments
101	3h23m.0	30°30'.0	158°.18	-21°.41	4.1	3.5	5.6	Mapped by
102	3 25.0	30 30.0	158.55	-21.16	6.9	5.4	3.4	Baran (1982)
103	3 25.0	30 00.0	158.87	-21.56	6.9	5.4	2.4	" "
104	3 26.5	31 10.0	158.40	-20.43	9.8	7.0	5.8	" "
105	4 03.0	24 32.0	169.52	-20.13	6.5	8.9	1.6	
106	4 19.7	19 25.0	176.34	-20.78	0.6	8.5	4.1	S238
107	4 24.5	18 45.0	177.66	-20.35	4.4	8.6	3.2	L1543
108	4 26.0	18 20.0	178.25	-20.34	3.1	7.6	1.6	L1546
109	4 28.5	18 00.0	178.92	-20.10	2.3	0.7	6.0	L1551; two
					7.4	6.6	2.0	components
110	5 17.7	-5 52.5	207.60	-22.94	0.9	10.3	3.2	S278
111	5 29.0	-5 25.0	208.54	-20.23	5.9	10.5	1.8	
112	13 54.5	-39 36.0	316.48	21.28	1.0	-5.7	1.9	CG12
113	15 17.1	-29 25.0	337.75	23.04	6.1	3.6	2.9	
114	15 18.5	-32 25.0	336.15	20.42	1.5	6.8	2.3	
115	15 29.2	-26 00.0	342.33	24.15	5.0	3.8	3.9	
116	15 29.4	-25 30.0	342.71	24.51	0.6	0.7	2.2	Two
					0.5	3.1	1.6	components
117	15 31.5	-25 40.0	343.00	24.08	0.6	--	--	
118	15 32.7	-24 33.0	344.01	24.77	0.5	3.7	2.0	
119	15 34.6	-28 33.0	341.61	21.41	3.0	3.1	1.7	
120	15 35.0	-24 52.0	344.23	24.19	1.2	3.7	2.9	
121	15 37.6	-24 47.0	344.78	23.87	4.7	-0.9	2.8	
122	15 37.6	-24 43.0	344.83	23.92	8.0	-0.6	2.5	
123	15 38.0	-27 00.0	343.29	22.12	3.3	1.1	2.3	Two
					5.3	3.5	2.1	components
124	15 38.4	-26 08.0	343.97	22.73	2.0	4.6	2.31	
125	16 12.0	-18 49.0	355.52	22.54	9.6	3.0	1.4	ρ Ophiuchus
126	16 16.3	-19 48.0	355.46	21.12	9.2	3.1	1.3	region
127	16 17.0	-20 00.0	355.42	20.87	4.0	3.0	1.4	" "
128	16 18.3	-20 05.0	355.57	20.58	10.4	3.1	1.7	" "
129	16 19.3	-19 33.0	356.16	20.76	8.5	3.7	1.3	" "
130	16 22.6	-19 25.0	356.81	20.26	9.2	2.5	2.5	" "
131	16 23.6	-16 45.0	359.16	21.79	4.7	0.6	2.6	
132	16 25.0	-15 00.0	0.85	22.64	1.6	1.1	1.4	
133	16 25.0	-17 00.0	359.18	21.38	5.6	0.1	1.2	
134	16 26.0	-16 03.0	0.14	21.79	6.9	0.4	1.4	
135	16 31.5	-14 05.0	2.69	21.98	6.8	-0.1	1.3	
136	16 31.3	-15 44.0	1.31	20.94	6.0	0.4	1.3	GGD 24
137	16 32.5	-12 10.0	4.49	22.95	3.6	-4.7	--	
138	16 33.0	-13 51.0	3.13	21.83	0.9	0.5	1.0	L106; two
					1.1	3.5	1.6	components
139	16 33.0	-8 40.0	7.66	24.93	0.8	2.4	1.4	L238
140	16 33.6	-13 51.0	3.22	21.72	0.9	-0.2	1.5	L106
141	16 34.5	-12 10.0	4.81	22.56	2.8	-1.5	1.5	L156
142	16 37.0	-13 55.0	3.70	21.02	6.2	-0.5	1.0	L121
143	16 45.0	-12 40.0	6.01	20.20	9.4	4.6	1.9	L190, L191
144	16 45.0	-12 00.0	6.59	20.58	7.9	3.6	2.2	L204
145	16 45.0	-9 50.0	8.49	21.84	7.6	3.8	1.3	L255
146	16 45.0	-9 30.0	8.78	22.03	6.9	3.1	1.6	L260
147	16 45.0	-12 50.0	5.94	20.00	6.4	3.5	2.4	L191
148	16 45.5	-11 00.0	7.54	21.06	7.4	2.8	--	L234
149	16 49.0	-11 10.0	7.92	20.27	2.7	4.0	1.8	L244
150	16 49.1	-9 18.0	9.57	21.31	4.8	3.1	1.5	
151	17 14.0	-0 02.0	21.52	20.93	2.2	-0.8	3.6	
152	19 10.2	-38 20.0	359.48	-20.47	4.1	6.0	2.2	Related to L229
153	19 11.2	-36 57.0	0.94	-20.20	3.3	6.0	2.1	" "
154	19 13.2	-36 43.0	1.32	-20.50	3.3	--	--	" "
155	19 17.4	-36 45.0	1.58	-21.30	3.4	5.2	1.9	" "
156	19 24.0	70 11.0	101.69	22.78	0.8	-10.7	1.4	
157	19 30.8	71 30.0	103.24	22.66	2.4	-1.3	1.6	
158	19 53.8	-14 17.0	27.19	-20.71	3.6	4.3	--	
159	19 55.8	-14 14.0	27.46	-21.13	4.0	4.6	1.7	S63
160	20 31.3	-1 33.0	43.96	-23.30	0.8	10.6	1.4	
161	20 53.0	81 00.0	114.65	22.52	0.4	-3.2	0.7	
162	21 00.0	77 20.0	111.67	20.10	2.9	-7.7	2.1	L1228
163	21 54.0	80 15.0	115.83	20.18	1.9	-8.0	3.4	Two
					4.5	-4.4	2.2	components
164	21 57.0	80 35.0	116.16	20.35	3.6	-5.2	2.2	
165	21 59.0	80 32.0	116.20	20.26	1.9	-8.6	2.7	Two
					3.1	-5.4	1.4	components
166	22 01.0	82 15.0	117.43	21.53	2.6	-4.8	1.7	

TABLE 2

CLOUDS $|b| \geq 25°$

[CO(J = 1–0)]

Complex	Cloud	α (1950)	δ (1950)	ℓ	b	T_A^* K	V_{LSR} km s^{-1}	Comments
1	1	$0^h08^m.0$	$20°21'.0$	110°.18	−41°.23	2.2	−6.0	
2	2	0 35.0	10 10.0	117.36	−52.28	1.7	−7.1	
3	3	1 13.1	16 32.0	131.28	−45.68	0.6	−7.6	
3	4	1 19.8	16 40.0	133.52	−45.31	0.7	−8.7	
4	5	1 49.3	10 49.0	145.96	−49.08	2.5	−9.8	
5	6	2 01.1	20 09.0	145.06	−39.35	5.8	6.8	
6	7	2 19.6	19 40.0	150.43	−38.07	5.1	4.5	
6	8	2 22.4	18 40.0	151.75	−38.68	1.7	5.2	
7	9	2 23.5	11 40.0	156.52	−44.71	1.3	−13.0	
8	10	2 44.1	−03 48.0	177.42	−53.80	1.0	3.4	
9	11	2 48.3	19 20.0	157.98	−35.06	4.1	−6.6	L1453, L1454
9	12	2 54.0	19 20.0	159.35	−34.32	5.7	−5.3	L1457, L1458
9	13	2 56.6	17 00.0	161.59	−35.89	4.4	−5.7	
10	14	3 09.0	19 50.0	162.44	−31.87	0.9	−2.2	
11	15	3 10.2	−09 35.0	191.67	−52.29	1.2	4.4	
12	16	3 17.7	10 30.0	171.68	−37.71	4.0	7.4	Large cloud
13	17	3 37.9	21 05.0	167.53	−26.61	2.4	7.9	
14	18	3 59.8	01 10.0	189.10	−36.02	7.0	8.0	L1569
15	19	4 13.3	06 51.0	186.04	−29.93	1.1	7.8	
16	20	4 33.0	−14 20.0	210.89	−36.51	6.8	0.3	L1642
17	21	4 59.4	−09 00.0	208.42	−28.39	6.7	4.8	
17	22	5 02.1	−08 20.0	208.08	−27.50	6.3	4.5	
18	23	7 32.3	46 48.0	171.83	26.72	0.9	−2.6	
18	24	7 34.2	46 28.0	172.27	26.97	1.5	−1.5	
19	25	8 01.2	46 00.0	173.75	31.48	2.5	−8.1	
20	26	8 02.8	60 43.0	156.42	32.60	2.4	−0.8	
21	27	8 43.8	72 48.0	141.33	34.45	3.0	0.6	
21	28	8 52.8	72 28.0	141.43	35.20	3.0	−0.7	
21	29	9 01.2	71 28.0	142.27	36.17	1.9	1.3	
22	30	9 24.2	70 38.0	142.20	38.22	1.8	2.7	
23	31	9 21.8	67 05.0	146.41	39.62	1.6	−0.7	
23	32	9 28.7	66 05.0	147.20	40.67	4.1	4.0	
24	33	15 37.2	−07 00.0	359.06	36.74	3.2	3.3	L1778, L1780
24	34	15 47.5	−05 42.0	2.36	35.66	1.5	3.2	
24	35	15 48.2	−01 32.0	6.57	38.13	1.4	1.1	
24	36	15 51.0	−04 30.0	4.18	35.75	5.8	2.0	L134
24	37	15 51.3	−03 00.0	5.70	36.62	5.1	2.3	L169, L183, L184
24	38	15 57.1	−01 33.0	8.22	36.34	6.7	0.8	S33
24	39	16 03.4	00 28.0	11.39	36.22	3.8	2.1	S36
25	40	16 08.4	21 57.0	37.57	44.67	4.4	3.5	S 73
26	41	16 48.3	60 05.0	89.61	38.42	2.6	−23.0	High velocity complex
26	42	16 50.1	60 55.0	90.59	38.04	1.3	−20.2	Noted by Mebold and
26	43	16 55.6	61 35.0	91.25	37.26	2.0	−23.2	Kalberla (1984)
26	44	16 58.5	62 15.0	91.99	36.80	1.8	−23.9	High velocity complex
27	45	19 59.3	−31 40.0	9.80	−28.02	2.4	6.7	
28	46	21 08.8	−09 55.0	40.54	−35.47	0.8	1.0	
28	47	21 10.9	−09 45.0	41.00	−35.86	0.7	1.2	
28	48	21 13.0	−10 24.0	40.57	−36.61	0.9	0.9	
29	49	21 25.3	12 05.0	64.74	−26.80	0.9	11.5	
30	50	21 51.2	12 40.0	70.02	−31.16	2.7	8.4	
31	51	22 55.7	−00 10.0	59.18	−40.13	0.9	1.1	
31	52	22 57.0	00 30.0	59.79	−40.19	0.8	−0.1	
32	53	22 58.5	23 57.0	92.97	−32.15	2.3	−11.3	
33	54	23 09.6	19 13.0	92.97	−37.54	2.9	−4.8	
33	55	23 05.9	14 49.0	89.19	−40.94	5.3	−8.1	Large filamentary complex; encompasses S122
34	56	23 23.2	33 12.0	103.08	−26.07	2.7	−5.1	
35	57	16 08.4	−06 56.0	5.80	30.84	1.7	−0.0	Observed in the CO (J=2-1) line only; S24

TABLE 3

CO(J = 2–1)

Complex	α (1950)	δ(1950)	l	b	T_A^* (K)	V_{LSR} (km s^{-1})	ΔV (km s^{-1})
2	00^{h}34^{m}3	+10°10′0	117°08	−52°26	0.6	−7.5	1.3
12	03 15.0	+11 00.0	170.63	−37.79	1.8	+6.8	1.2
20	08 05.5	+61 13.0	155.81	+32.92	0.9	−0.5	0.9
	08 02.8	+60 43.0	156.42	+32.60	1.1	−0.8	1.9
	08 02.8	+60 33.0	156.62	+32.61	1.0	−0.5	1.4
21	08 52.8	+72 08.0	141.81	+35.32	0.8	−1.1	0.7
	08 55.0	+72 08.0	141.74	+35.47	0.5	−0.8	1.2
22	09 24.2	+70 38.0	142.20	+38.38	1.2	+2.8	1.6
28	21 13.0	−10 24.0	40.57	−36.61	0.9	+0.9	2.3
	21 12.3	−10 04.0	40.85	−36.30	0.4	+0.8	2.9
33	23 05.9	+14 29.0	88.96	−41.22	1.9	−5.6	3.5
	23 07.3	+14 49.0	89.57	−41.11	2.8	−4.9	1.8
	23 04.5	+14 09.0	88.35	−41.33	1.9	−6.1	3.3
35[a]	16 08.4	−06 56.0	5.80	+30.84	1.7	−0.0	0.8

[a] S24.

rated antenna temperature ($\int T_A^* dv$) present if the object was mapped, and to the original search catalog position if the object was not mapped. Columns seven through nine list the antenna temperature, the LSR velocity, and comments on individual clouds. Results of the ^{13}CO and CO(J = 2–1) observations are listed in Tables 3 and 4 for the sampled lines of sight within some of the clouds.

b) Distribution of Objects

The spatial distribution in galactic coordinates of our detections is shown in Figure 1. Some of the detections appear to be the southernmost parts of the Taurus and Perseus molecular clouds at $b \leq -20°$ and l = 155–180°; the northernmost concentrations of molecular gas in the dark clouds of Scorpius and Ophiuchus located at l = 355–10° and $b \geq 20°$; and the region at $l \approx$ 320–345° and $b \geq 20°$ to which Blaauw (1982) has called attention as a possible source of molecular material. There is a gap in the distribution of clouds in the northern hemisphere from $l \approx 180°$ to $l \approx 340°$ which is coincident with a drop in H I column density out to large distances discussed by Paresce (1984).

For the complexes at $|b| \geq 25°$, 29% are at northern lati-

TABLE 4

Complex	α(1950)	δ(1950)	l	b	T_A^* (K)	V_{LSR} (km s^{-1})	Δv (km s^{-1})
			13CO(J = 1–0)				
12	03^{h}15^{m}0	+11°00′0	170°63	−37°79	0.4	+6.7	0.6
	03 15.0	+10 50.0	170.78	−37.91	0.4	+6.8	0.6
16	04 33.0	−14 10.0	210.70	−36.44	1.2	+0.8	0.6
	04 33.0	−14 20.0	210.89	−36.51	4.0	+0.3	0.9
	04 33.0	−14 30.0	211.08	−36.58	2.9	+0.3	0.5
	04 33.0	−14 40.0	211.27	−36.64	0.9	+0.4	0.7
	04 33.0	−14 50.0	211.46	−36.71	0.2	+0.5	1.1
20	08 05.5	+61 13.0	155.81	+32.92	0.1	−0.5	0.9
	08 02.8	+60 33.0	156.62	+32.61	0.2[a]	−1.1	0.5
					0.3[a]	−0.3	0.4
22	09 24.2	+70 38.0	142.20	+38.22	0.2	+2.6	2.4
	09 22.1	+71 38.0	141.19	+37.59	0.6[a]	+1.7	0.6
					0.3[a]	+2.5	0.3
25	16 07.7	+22 07.0	37.72	+44.87	0.2	+3.1	0.8
	16 08.4	+21 57.0	37.57	+44.67	0.7	+3.5	0.7
	16 09.1	+22 07.0	37.86	+44.56	0.4	+3.0	0.4
26	16 45.6	+60 25.0	90.12	+38.68	0.1[a]	−25.2	0.8
					0.1[a]	−23.7	0.8
33	23 05.9	+14 49.0	89.19	−40.94	1.5	−7.7	1.7
	23 05.9	+14 29.0	88.96	−41.22	0.3	−5.9	3.4
			13CO(J = 2–1)				
	08^{h}02^{m}8	60°33′0	156°62	+32°61	0.2	−0.0	1.6

[a] Two components.

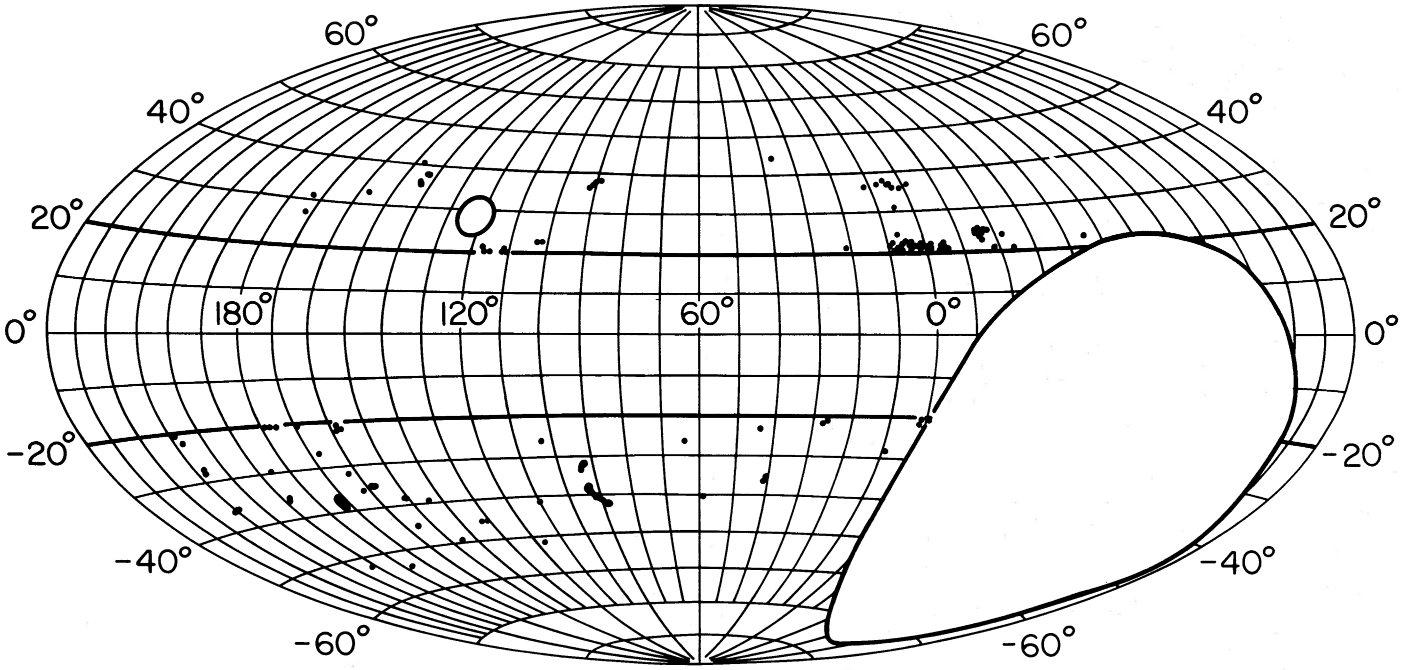

FIG. 1.—Distribution on the sky in Galactic coordinates of the high-latitude molecular clouds detected at $|b| \geq 20°$. Blank areas could not be observed with the Texas instrument.

tudes, 71% are at southern latitudes. This difference does not appear to be due to observational selection, and it is consistent with the stellar data which imply that the Sun is somewhat above the Galactic midplane. Assuming a Gaussian latitude distribution for the clouds, and a scale height of 75 pc (see § IV*a*), the north-south asymmetry in the distribution implies that the Sun is ~ 30 pc above the midplane. This value is consistent with the value found from Population I Cepheids (Blaauw 1960).

Seventy percent of the complexes detected at $|b| \geq 25°$ are located within 1° of a Lynds bright nebula (LBN; Lynds 1965). Six out of 35 are near a LBN which Lynds denotes as brightest on the blue plates, ten are near LBNs which are deemed of equal brightness on both plates, four are near LBNs which are brighter on red plates, and four are near LBNs visible only on red plates. The high-latitude LBNs which are prominent on the blue plates or are equally bright on both plates are probably dusty nebulae reflecting the starlight of the galactic plane (van den Bergh 1966; Sandage 1976). Our observations demonstrate that some of these regions also contain molecular material. The distribution of sources with respect to the absolute value of the galactic latitude is given by Figure 2.

For the entire survey, the detections range in peak intensity from $T_A^* = 0.5$–11.3 K. For the clouds at $|b| \geq 25°$ the peak CO($J = 1$–0) intensity ranges from $T_A^* = 0.6$–7.0 K with a mean 2.8 K. Most of these sources show relatively strong CO lines; only five of 56 clouds have peak temperatures less than 0.9 K. Of these five objects, two are not mapped (clouds 3 and 4), and the other three are small, individual objects in well-defined complexes (clouds 46, 47, and 52).

The typical line widths (ΔV) are relatively narrow; 1–1.5 km s^{-1} FWHM. This contrasts with line widths of 3–5 km s^{-1} which are typical of local giant molecular clouds (see, e.g., Blitz 1978). In some of the clouds that have been mapped, a few lines of sight have line widths as small as 0.25 km s^{-1}. These line widths are the narrowest yet observed for CO. However, even these lines are supersonic, since the thermal line width for a CO cloud at 10 K is 0.05 km s^{-1}. One of the objects, cloud 12, has very broad lines, $\Delta V > 5$ km s^{-1}. Such broad CO lines are generally seen only in regions of

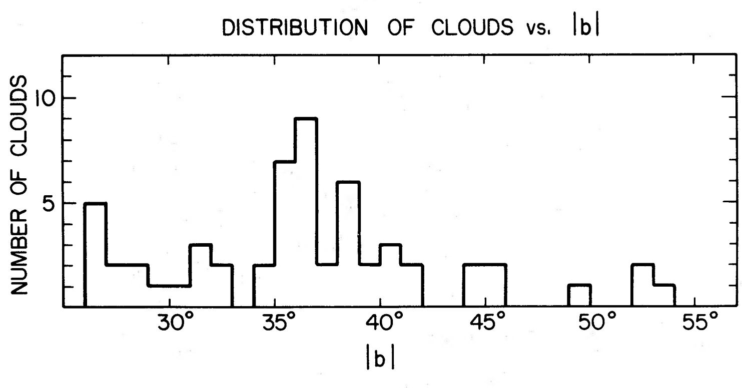

FIG. 2.—Distribution of individual clouds with respect to absolute value of Galactic latitude

active star formation or in regions where several independently moving fragments lie along the line of sight.

c) *Nondetections*

CO emission was searched for and not detected in the following regions where the presence of molecular gas had been expected: (1) the five high Galactic latitude clouds detected by *IRAS* (Low *et al.* 1984) and identified as A, B, C, D, and X; (2) two regions which show ultraviolet excess at high Galactic latitudes (Paresce, Jakobsen, and Bowyer 1983); and (3) three OH clouds denoted A, C, and E by Verschuur (1971). None of these areas showed CO emission at a $T_A^* > 0.3$ K. Using the CO/H_2 conversion factor of § IV*b* and using a typical line width of 1.5 km s^{-1}, the nondetections imply upper limits for the molecular hydrogen column density of less than 1.2×10^{20} cm^{-2}.

d) *Mapping*

The mapped complexes are shown in Figure 3. The objects range from small, individually separated cloudlets to large complexes spanning many degrees. In two cases the core regions of the molecular clouds were observed with full beamwidth sampling revealing structure even on size scales down to the resolution limit of the instrument.

The 23 complexes we mapped cover an area >30.1 deg^2, while the complex which incorporates L134 mapped by Montani, Morris, and Thaddeus (1985) contributes an additional 3.8 deg^2 for a mapped total of 33.9 deg^2. If the other 10 clouds not mapped have the same mean projected area as the mapped clouds, the total area of the clouds in our sample is 48 deg^2. The fraction of the sky at $|b| \geq 25°$ accessible from MWO is 0.47; therefore, one expects only one random line of sight in approximately 400 will produce a CO detection. This is in good agreement with the extrapolation in Paper I based on significantly less mapping data.

Some of the sources are filamentary and extend over several degrees. The largest of these structures is complex 33, which includes clouds 54 and 55 (see Fig. 3). Mapping reveals that these clouds, which are elongated almost perpendicular to the galactic plane, span more than 9° and are as yet incompletely mapped at the northern end (cloud 54). Cloud 53 is also filamentary with its southern end only 2° from cloud 54. Further sampling of this region may reveal even more extensive molecular emission.

In the northern hemisphere, the group centered on cloud 36 ($l = 4\overset{\circ}{.}2$, $b = 35\overset{\circ}{.}8$; L134) consisting of clouds 33–39 also stretches over 10°. However, the molecular material is clumped in distinct, centrally condensed entities rather than in a single connected filament. The main clouds, 36 (L134) and 33 (L1778), have been extensively studied (e.g., Mahoney, McCutcheon, and Shuter 1976; Tucker *et al.* 1976; Mattila and Sandell 1979; Mattila 1979; Clark and Johnson 1981). Clouds 33 and 36–39 have been mapped in CO($J = 1$–0) by Montani, Morris, and Thaddeus (1985). Clouds 34 and 35 are small, distinct objects found during our survey near the larger clouds. These small clouds may be part of more small molecular condensations in the area.

The filamentary structures of molecular material observed by Morris, Montani, and Thaddeus (1980) in the Orion region appear to be similar to the structures described above. The size and morphology of many of the clouds we have detected are similar to the "high-latitude cirrus" detected by *IRAS* (Low *et al.* 1984). Using a gas to dust ratio of 100, and dust temperatures typical of dark clouds (~25–40 K), the expected 100 μm infrared flux from these objects is comparable to the flux detected by *IRAS* for the cirrus.

In addition to the above objects, two complexes merit comment: Cloud 16 and clouds 41–44. Cloud 16 is a large region greater than 5.5 deg^2 in spatial extent and incompletely mapped at its northern edge. There are two regions within the contiguous boundary of the cloud where the antenna temperature was less than 0.3 K. Future observations will determine whether these are actual holes in the cloud or whether they are "filled in" by atomic hydrogen. Clouds 41–44, constitute the high velocity complex. The four individual clouds in this complex all have velocities ≤ -20 km s^{-1}, 4.5 times the value of the velocity dispersion of the ensemble. Cloud 41 has been studied in H I by Goerigk *et al.* (1983), and CO has been independently detected in it by Mebold and Kalberla (1984).

Maps are not included for Clouds 21, 22, and 50 because at 20′ sampling intervals, molecular emission was detected only at the positions listed in Table 2.

e) *Correlation with* H I

Using the Heiles and Habing (1974) high-latitude H I survey as an indicator of N(H I) in the general direction of the clouds, it is clear that there is an H I emission feature at the position and velocity of the high-latitude CO. Even the complex at -24 km s^{-1} has an H I counterpart. Although there is no direction in which CO is detected without associated H I, the velocity of the peak of the CO emission does not always coincide with the velocity of the peak of the 21 cm line. It is important to note that although virtually all clouds show concentrations of H I, not all concentrations of H I at high Galactic latitudes are associated with concentrations of molecular gas.

A comparison of H I and H_2 column densities indicates that H_2 is usually dominant. Because the Heiles and Habing (1974) survey samples the H I along the entire line of sight while the CO is more spatially confined, the ratios of $N(H_2)/N$(H I) should be lower limits to the corresponding ratio for volume density. Ratios $N(H_2)/N$(H I) are typically 2–3, but values as high as 9 and as low as 0.2 are observed. Figure 4 is a plot of $N(H_2)$ versus N(H I) for the high-latitude clouds, showing the dominance of $N(H_2)$, and with no apparent correlation between the two quantities.

f) *Star Formation*

Five of the clouds have compact nebulous emission near the CO peaks. In one case (cloud 2) the nebulosity is clearly a galaxy; in another (cloud 20), the nebulosity is associated with a T Tauri star near the CO intensity maximum. The three remaining objects may be emission or reflection nebulae associated with the early stages of star formation. Because of the proximity of these clouds (see § IV*a*) the stars forming in the high-latitude molecular clouds are likely to be the star-forming sites closest to the Sun. If so, observations of these objects could provide the best angular resolution for the study of star formation yet attained. The positions of the nebulosities are shown on the maps of the individual clouds. We comment on the regions individually below.

Cloud 2.—A typical small cloud which shows the galaxy IC 35 immediately next to its peak contour. That this galaxy can be seen so clearly through the molecular cloud is independent evidence for the small values of the extinction derived in Paper I and discussed in § IV*c*.

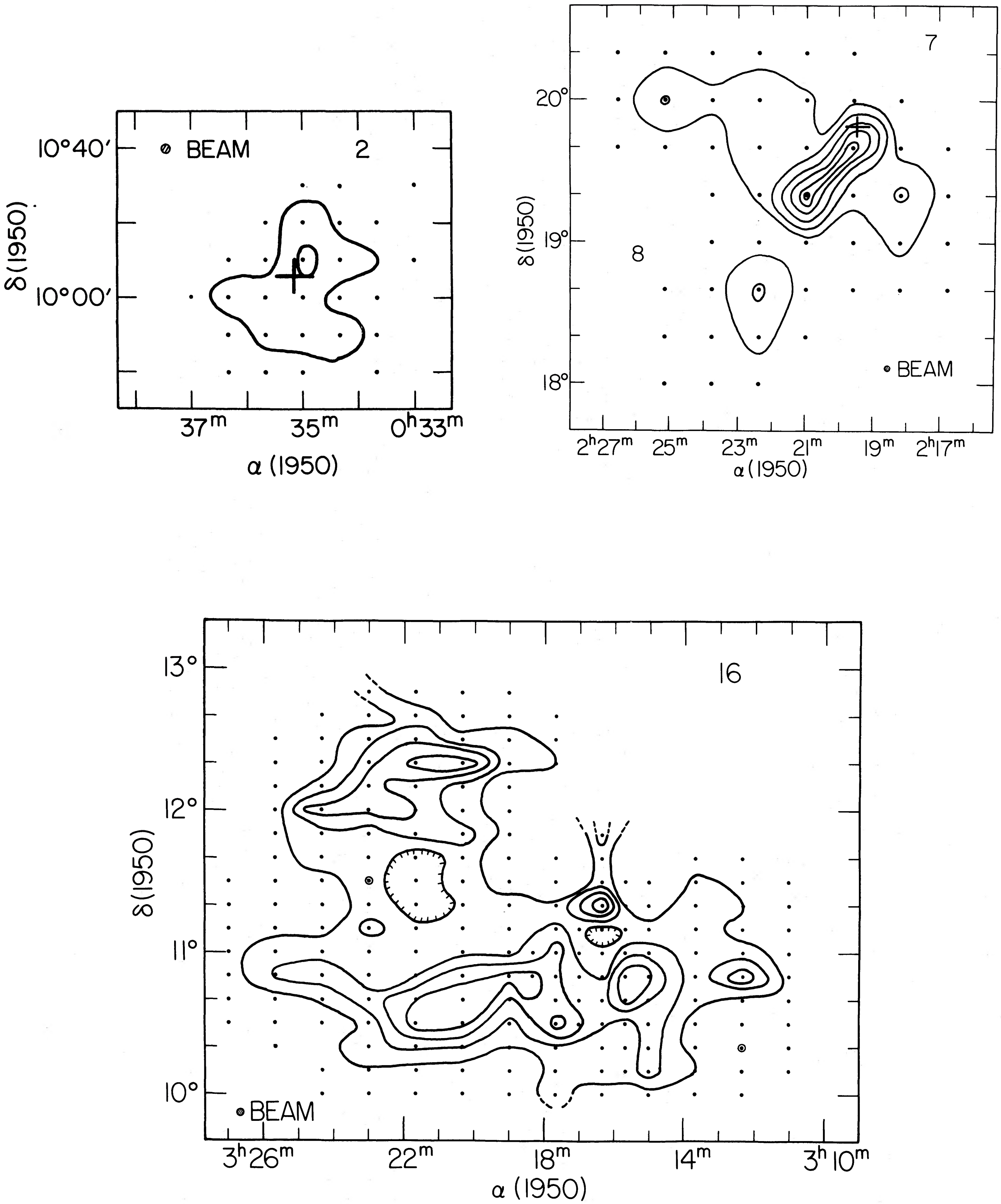

FIG. 3.—Maps of the peak T_A^* of the clouds. The lowest contour is at 0.5 K and each succeeding contour is greater by 1 K. Dots indicate all the observed positions. Crosses indicate nebulous objects described in the text. Clouds 21, 22, and 50 consist of single points at 20′ resolution.

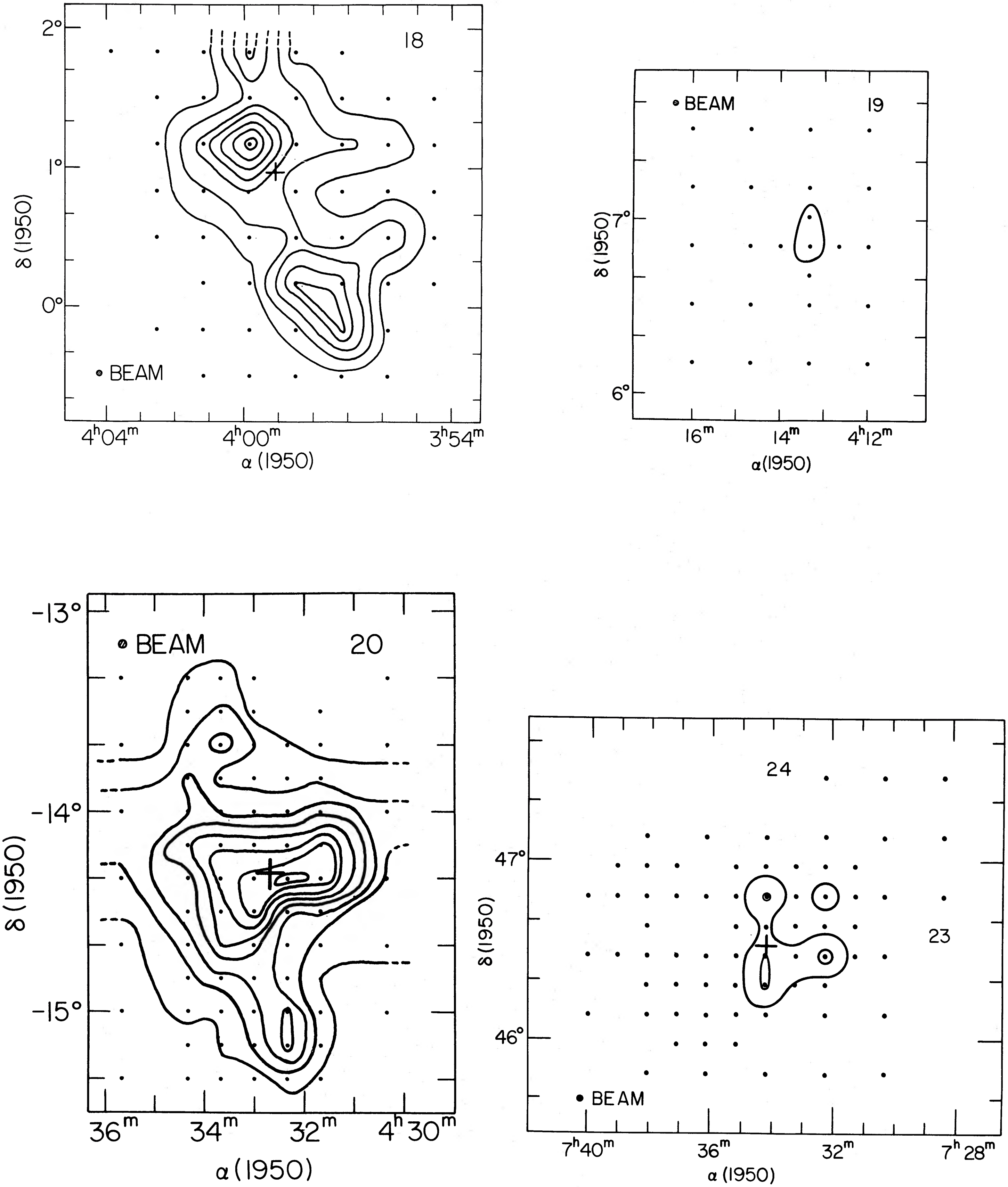

FIG. 3.—*Continued*

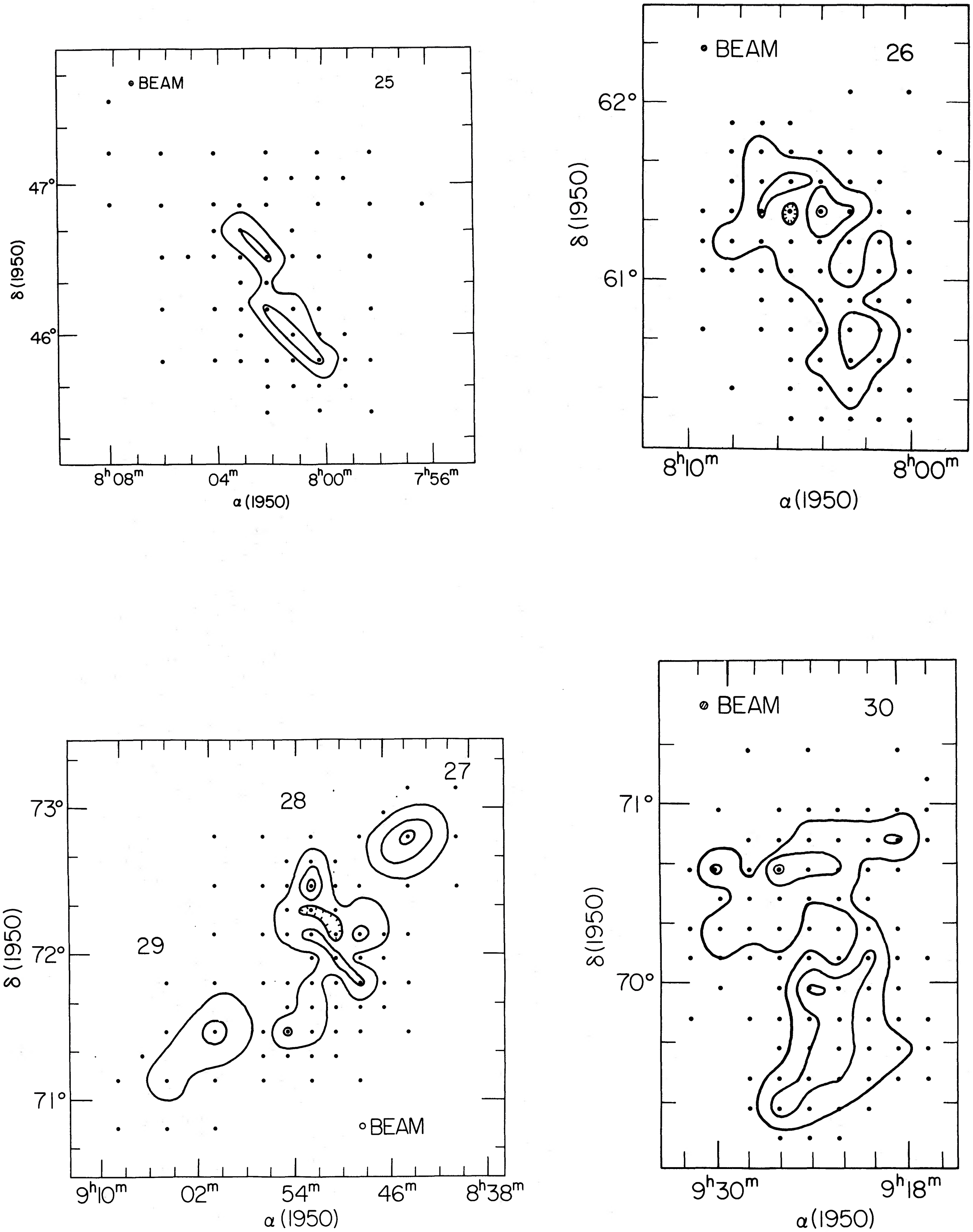

FIG. 3.—*Continued*

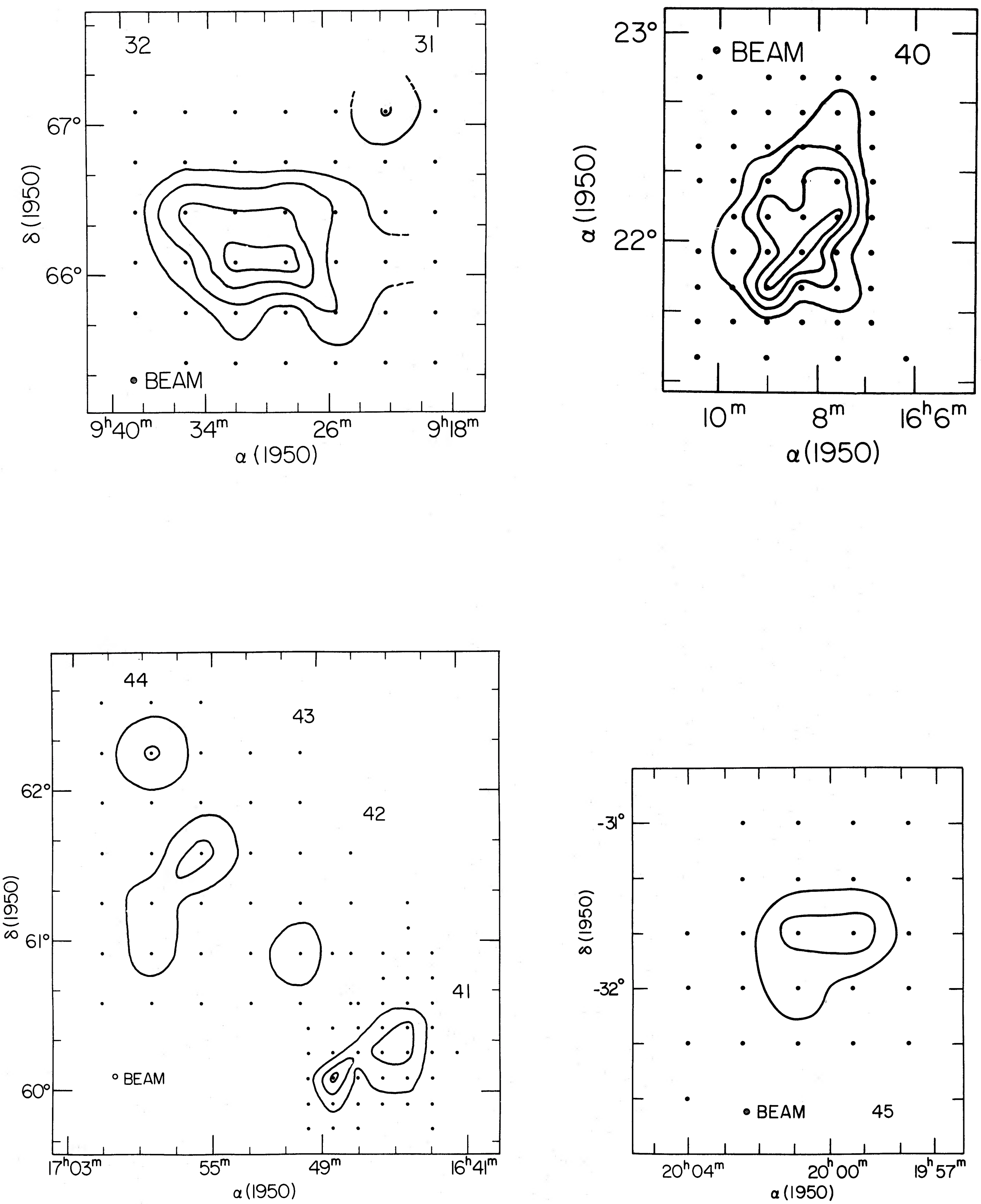

FIG. 3.—*Continued*

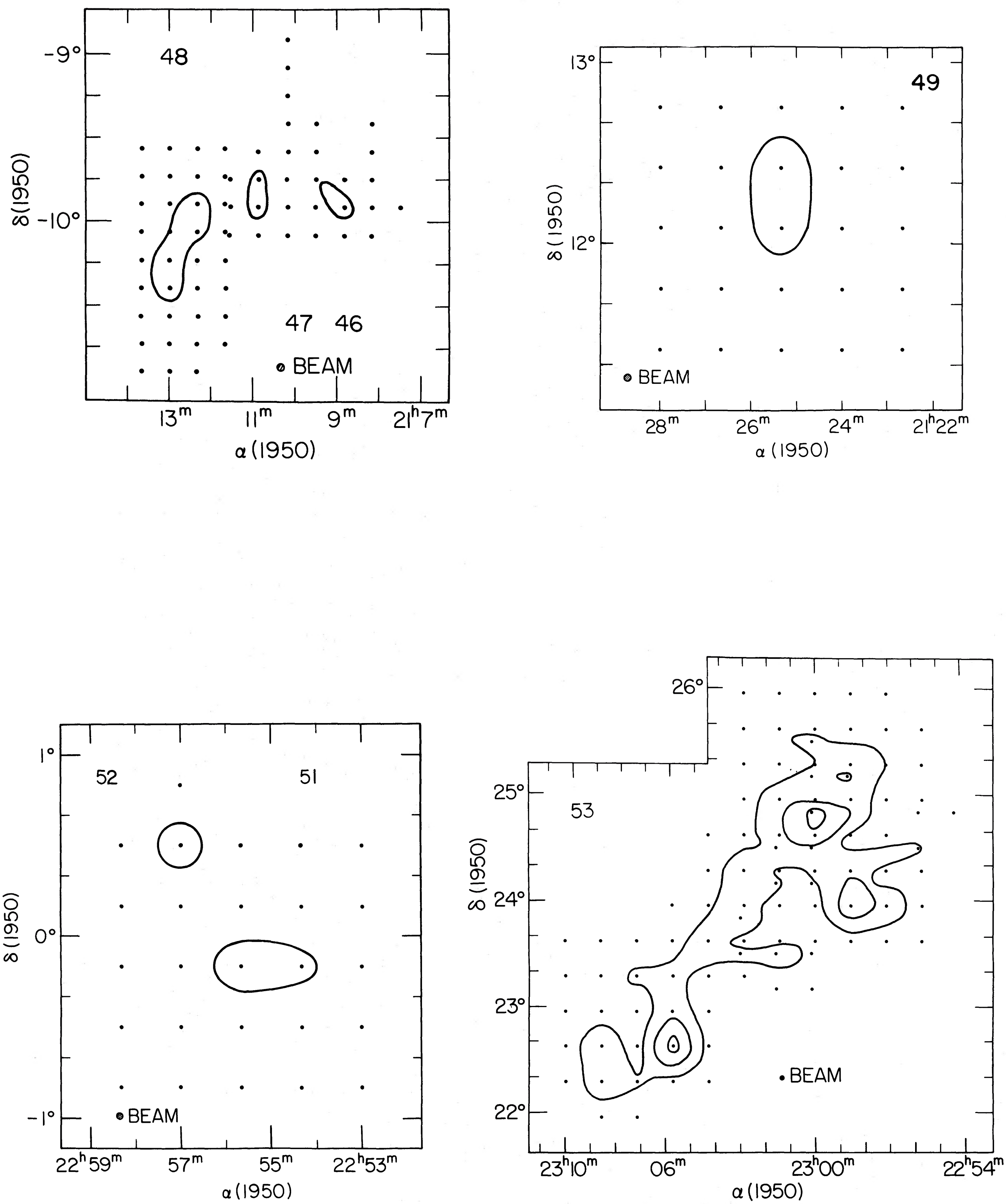

FIG. 3.—*Continued*

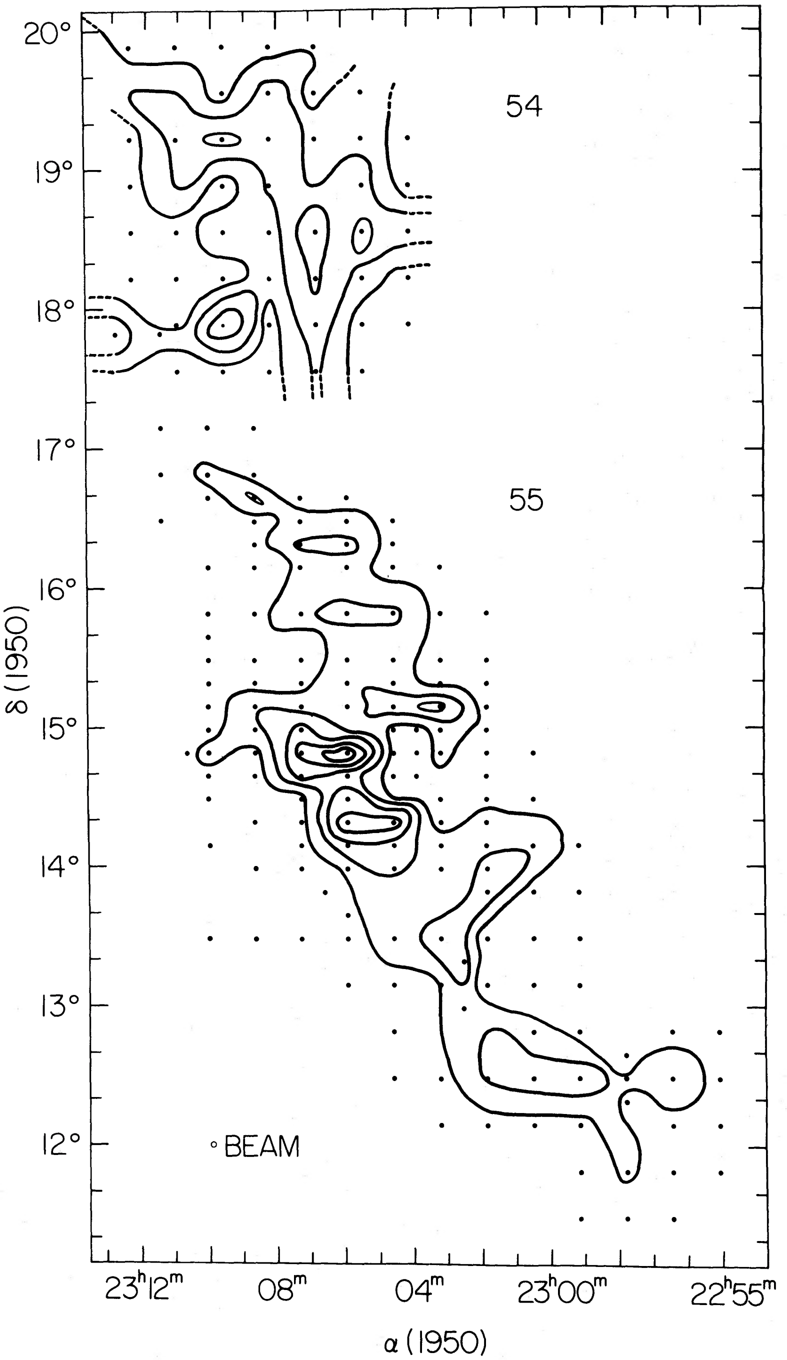

FIG. 3.—*Continued*

Clouds 7 and 8.—Two obviously related objects. Cloud 7 shows a core region where the antenna temperature reaches 6.5 K. Near the central condensation of cloud 7 at $\alpha(1950) = 2^{h}19^{m}30^{s}$ and $\delta(1950) = 19°48'30''$, the POSS prints show a very small, faint, fuzzy patch.

Cloud 18.—Also known as L1569, it is elongated perpendicular to the Galactic plane. This cloud shows two condensed regions and probably extends to the north of the region mapped. There is a stellar object surrounded by nebulosity near the central condensation at $\alpha(1950) = 3^{h}59^{m}6^{s}$ and $\delta(1950) = 0°57'30''$ which is brighter on the red print than on the blue print. It appears similar to the object in cloud 7.

Cloud 20.—Also known as L1642, it is incompletely mapped. The cloud has a central condensation and a nebulous object near the area of peak emission of the cloud at $\alpha(1950) = 4^{h}32^{m}44^{s}.7$ and $\delta(1950) = -14°19'36''$. This cloud has been extensively observed and mapped in OH and CH by Sandell *et al.* (1981), in H_2CO by Goss *et al.* (1980), and in $CO(J = 2-1)$ by de Vries *et al.* (1984). The nebulous object near the central condensation has been referred to as a "cometary nebula" by Sandell *et al.* (1981). The associated stellar object has recently been shown to be a T Tauri star (Sandell, private communication). Thus at least some of the high-latitude clouds form stars.

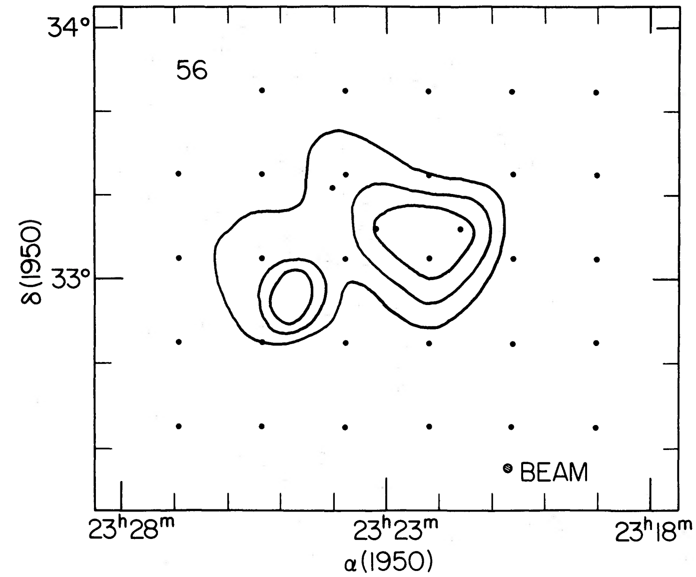

FIG. 3.—*Continued*

Clouds 23 and 24.—A typical example of a small, fragmented complex with a nebulous object directly at the peak of cloud 23. This object is classified as galaxy UGC 03935 (Nilson 1973), but close examination reveals nebulosity surrounding a star-like core which is much brighter on the red prints than on the blue.

g) Velocity Structure

Many of the clouds have a complex velocity structure. Twelve of the 23 complexes which have been mapped show multiple velocity components along a given line of sight. Figure 5 shows some examples of this. Virtually all the complexes where detections were made along more than two lines of sight show a rich velocity structure. In clouds 53 and 55 the velocity components are separated by as much as 10 km s^{-1}. Based on the velocity information in our spectra, we derive a velocity dispersion for each individual cloud which reflects the internal kinetic energy of each cloud.

Each spectrum has a Gaussian profile fitted to it with the centroid representing the line-of-sight velocity of the clump within the beam of the telescope. If the column density of a clump is proportional to the velocity-integrated antenna temperature, then the square of the mass-weighted one-dimensional velocity dispersion σ_v(int) is given by

$$\sigma_v^2(\mathrm{int}) = \left(\frac{N}{N-1}\right) \frac{\sum_{i=1}^{N} (T_A^* \Delta V)_i (v_i - \bar{v})^2}{\sum_{i=1}^{N} (T_A^* \Delta V)_i} . \qquad (1)$$

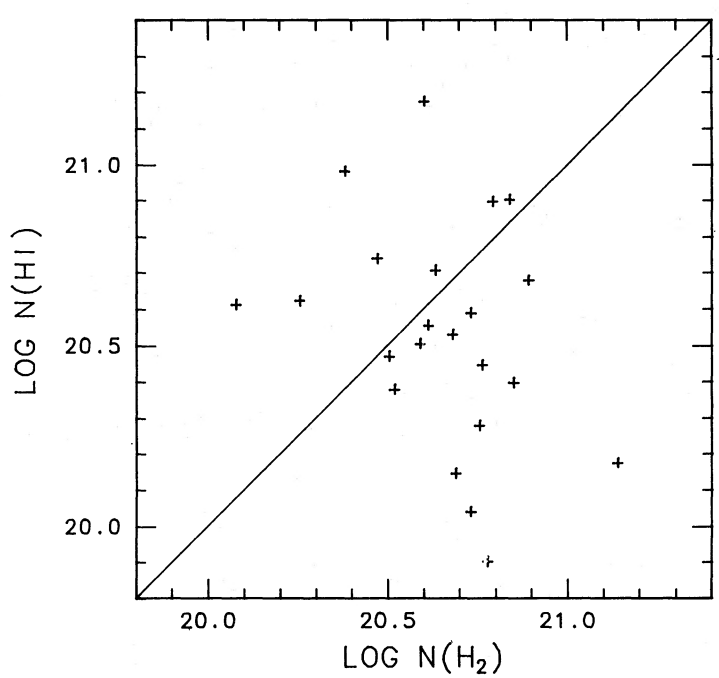

FIG. 4.—Plot of log $N(H_2)$ vs. log N(H I). The diagonal line represents points of equal column density.

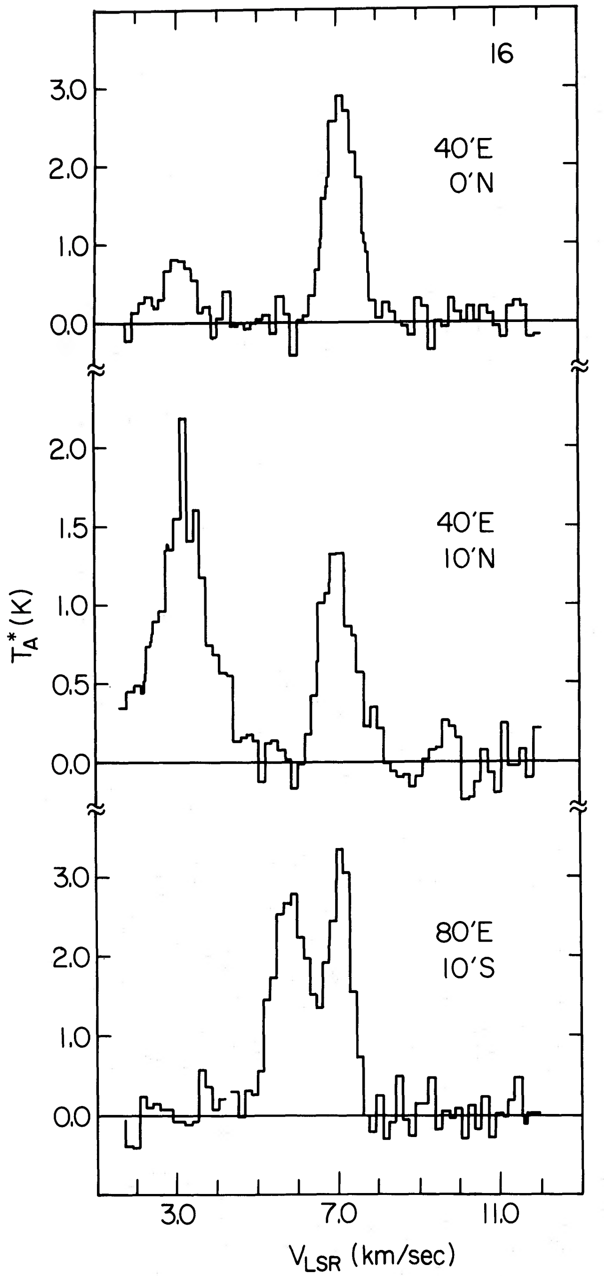

FIG. 5.—Several examples within a cloud which show multiple components along the line of sight.

The velocity centroid of a clump is denoted by v_i, N is the total number of individual profiles fit within a cloud, and $\bar{v}$ is the intensity weighted mean LSR velocity of all the points in the cloud. The range of σ_v(int) for all the clouds is 0.11 km s^{-1} to 3.12 km s^{-1} and the value for each mapped cloud is listed in Table 5.

h) Velocity Dispersion of the Ensemble

To properly determine the one-dimensional velocity dispersion of the ensemble of clouds, σ_v(c-c), it is necessary to account for both the mass of each cloud and for the effects of Galactic differential rotation.

To account for differential rotation, we use the intensity-weighted mean velocity v_{LSR} of each complex listed in Table 5 and subtract the component of the velocity expected from differential rotation $v_{diff} = Ad \sin(2l) \cos b$, where A is the local Oort A constant and d is the distance to the complex (assumed for all to be 100 pc; see § IV*a*). Thus each complex has a corrected velocity v_0 such that

$$v_0 = v_{LSR} - v_{diff} \ .$$

Knowing the mass of each complex requires knowledge of the distance to it, a quantity not yet available. Instead of using the mass, each v_0 is weighted by the product of the area of each cloud and its mean velocity-integrated antenna temperature. This is roughly equivalent to weighting by the mass if all the clouds are at the same distance. Thus,

$$\sigma_v^2(\text{c-c}) = \left(\frac{N}{N-1}\right) \frac{\sum_{j=1}^{N} (T_A^* \Delta V)_j A_j (v_j - \bar{v}_0)^2}{\sum_{j=1}^{N} (T_A^* \Delta V)_j A_j} \ , \qquad (2)$$

where $(T_A^* \Delta V)$ is the mean integrated antenna temperature of the jth complex, A_j is the projected area of the jth complex, and $\bar{v}_0$ is the weighted mean velocity relative to the LSR of the entire ensemble corrected for Galactic differential rotation.

Although we did not fully map the L134 complex, we use a map of the region (Montani, Morris, and Thaddeus 1985) to determine the weighting factors for clouds 33–39. We do not include the high-velocity complex because its very high velocity indicates that it may not belong to the ensemble of clouds.

By this method, the velocity dispersion of the ensemble is 5.6 ± 1.2 km s^{-1} and the mean velocity with respect to the LSR is 0.13 ± 0.11 km s^{-1}, insignificantly different from 0. The correction for the differential Galactic rotation amounts to less than 0.1 km s^{-1} in σ_v(c-c). We can estimate the effect of weighting by the mass by calculating an unweighted σ_v'(c-c), where we use the weighted velocity for each complex but we do not weight the complexes by the integrated antenna temperature or area. In this manner σ_v'(c-c) = 5.3 km s^{-1}, which is within 1 σ uncertainty of the weighted dispersion. In any event, σ_v(c-c) is significantly less than the value of $9.0^{+1.1}_{-1.2}$ km s^{-1} obtained by Stark (1984) for small dark clouds of masses 10^2 $M_\odot$ to 10^4 $M_\odot$. Liszt, Burton, and Xiang (1984) obtain a value of 4.5 km s^{-1} for σ_v(c-c) of inner Galaxy molecular clouds, but their analysis may be skewed to higher mass clouds. In addition, our value of σ_v(c-c) is marginally smaller than the value of 6.9 ± 0.4 km s^{-1} obtained by Belfort and Crovisier (1984) from 21 cm line measurements of nearby H I clouds.

A longitude velocity plot of the clouds (see Fig. 6) indicates that the distribution of velocities may not be random. There are, for example, no clouds in the first quadrant with negative radial velocities. The lack of clouds at $355° > l > 205°$ makes the plot difficult to interpret.

i) Isotopic Abundances and Excitation Temperatures

The ratio of $\int T_A^*(12)dv / \int T_A^*(13)dv$, hereafter $I12/I13$, was calculated for those lines of sight in clouds where we have ^{13}CO values (see Table 4) and ranges from 2.3 to 18.4 with a mean of 10.3 ± 1.2. This value is in agreement with the value found for $R = R_0$ from the Galactic survey of Liszt, Burton, and Xiang (1984). In most cases, the ^{13}CO emission lines are narrower, but in four directions the two isotopes have the same width, within the uncertainties of the measurement. These observations imply that CO is still optically thick in the high-latitude clouds, but not as thick, on average, as the molecular clouds in the inner Galaxy.

Because CO lines are generally heavily saturated, the ^{13}CO emission lines offer a better chance to identify separate clouds.

TABLE 5

Complex	Cloud	σ_v(int)	v_{LSR}	σ_v(vir)	$\frac{\sigma_{int}}{\sigma_{vir}}$	A_v(cloud)	A_v(peak)
2...........	2	0.89	−7.29	0.06	14.8	0.6	1.1
6...........	7, 8	0.57	+4.63	0.11	5.2	1.1	3.2
12...........	16	0.85	+6.85	0.15	5.7	1.3	2.5
14...........	18	1.17	+9.88	0.16	7.3	1.2	2.5
15...........	19	0.99	+7.84	0.04	24.8	0.8	0.9
16...........	20	0.39	+0.63	0.14	2.8	0.7	3.0
17...........	21, 22	0.21	+4.67	0.13	1.6	1.5	1.8
18...........	23, 24	0.85	−1.65	0.08	10.6	0.7	1.3
19...........	25	0.56	−8.12	0.09	6.2	0.7	1.2
20...........	26	0.60	−0.41	0.09	6.7	0.5	1.1
21...........	27–29	2.02	−0.07	0.11	18.4	0.6	1.3
22...........	30	0.92	+2.06	0.12	7.7	0.8	1.6
23...........	31, 32	2.27	+2.20	0.15	15.1	0.9	1.7
24...........	33–39	...	+2.16[a]	...	...	...	...
25...........	40	0.25	+3.24	0.08	3.1	0.7	1.4
26...........	41–44	1.49	−23.27	0.11	13.5	0.7	1.1
27...........	45	0.11	+6.76	0.11	1.0	[b]	[b]
28...........	46–48	0.20	+0.98	0.06	3.3	0.6	0.7
29...........	49	0.78	+10.99	0.07	11.1	0.5	0.5
30...........	50	[c]	+8.36	...	...	0.8	0.8
31...........	51, 52	0.64	+0.60	0.04	16.0	0.4	0.5
32...........	53	3.12	−5.70	0.14	22.3	0.6	1.1
33...........	54, 55	2.09	−5.53	0.21	10.0	1.1	4.8
34...........	56	1.56	−7.15	0.18	8.7	1.6	3.4

[a] Estimated from map of Montani, Morris, and Thaddeus 1985.
[b] No N(H I) information available.
[c] Consists of only one point at 20′ resolution.

Two of the 19 lines of sight which show a single component in CO have two distinct components in ^{13}CO (see Fig. 7). ^{13}CO line splitting therefore appears to be a common phenomenon in the high-latitude clouds and indicates that the velocity structure of the clouds is even more complex than is indicated by CO mapping.

Observations of the CO(J = 1–0) and the CO(J = 2–1) transitions along the same lines of sight allow us to calculate the

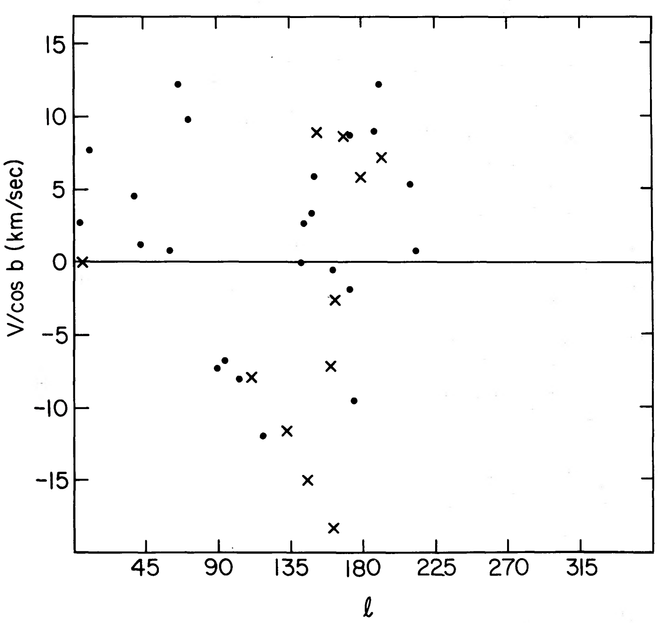

FIG. 6.—Longitude-velocity plot of the $\bar{v}$ for the complexes. A dot indicates a mapped complex and a cross indicates a region where we have velocity information for just one line of sight.

excitation temperatures for those particular positions in the clouds. Assuming $\tau \gg 1$, the observed line temperature (T_L) can be expressed in terms of the excitation temperature (T_x) and the background temperature (T_{BB}) as

$$J(T_L) = J(T_x) - J(T_{BB}) ,$$

where J is the Planck function.

Solving this equation for the excitation temperature yields, for CO(J = 1–0),

$$T_{x(1-0)} = 5.53\left[\!\left[\ln\left\{1 + \frac{1}{[\exp(5.53/T_L) - 1]^{-1} + 0.148}\right\}\right]\!\right]^{-1} , \quad (3)$$

and for CO(J = 2–1),

$$T_{x(2-1)} = 11.06\left[\!\left[\ln\left\{1 + \frac{1}{[\exp(11.06/T_L) - 1]^{-1} + 0.017}\right\}\right]\!\right]^{-1} . \quad (4)$$

In both instances, T_L is obtained from our data by using $T_R = T_A^*/\eta_{FSS}\eta_c$, where $\eta_{FSS}\eta_c \approx 0.8$ for both CO(J = 1–0) and CO(J = 2–1) for sources greater than 30′ in diameter (Mundy, private communication). For these calculations, the CO(1–0) transitions are scaled by a factor of 1.25 to make T_A^* conform to Orion = 76 K. The results, plotted in Figure 8, imply that the excitation temperatures derived from the J = 2–1 line are somewhat lower than those derived from the J = 1–0 line, suggesting that the J = 2–1 line is subthermally excited.

IV. DERIVED PROPERTIES

a) Distance

A statistically determined distance to the complexes at $|b| \geq 25°$ was determined in Paper I. If the molecular gas layer

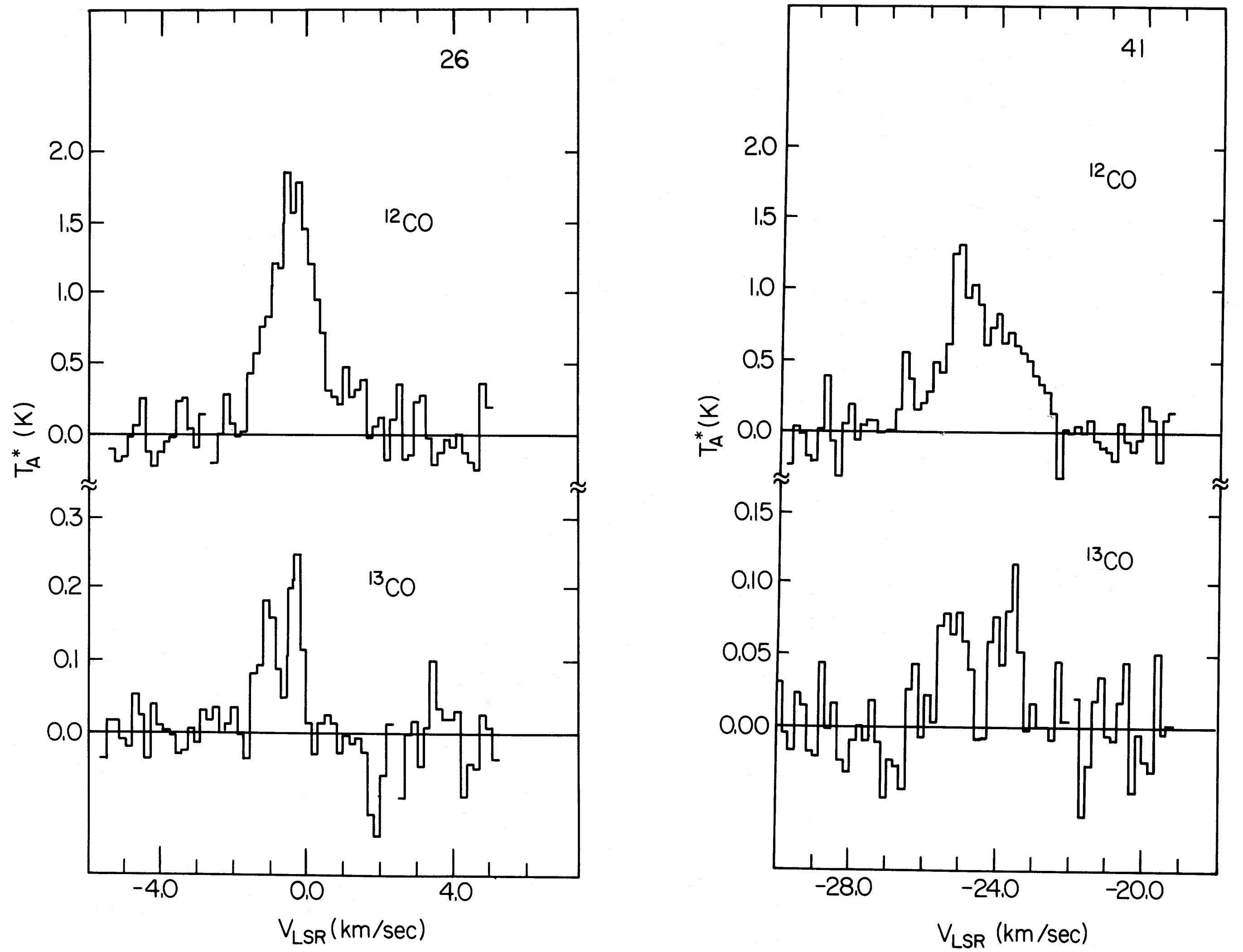

FIG. 7.—Examples of clouds which have a single CO component along a line of sight and double components in ^{13}CO along the same line of sight.

is distributed in the manner delineated in Paper I, then the expectation value for the height above the plane $\langle z \rangle$ is given by $0.798\ \sigma_z$, where σ_z is the Gaussian scale height of the gas. The scale height of the molecular gas in the solar vicinity must therefore be obtained.

Following van der Kruit (1981) we obtain a relation for $(z_{1/2})_{\rm CO}$, the height at which half the CO per unit area lies between $(z_{1/2})_{\rm CO}$ and $(-z_{1/2})_{\rm CO}$:

$$\langle z_{1/2} \rangle_{\rm CO} = \frac{1.7 \langle v_z^2 \rangle_{\rm CO}^{1/2}}{[\pi G \sigma_s(R_0) z_0]^{1/2}} . \qquad (5)$$

We will take canonical values for local stellar scale height z_0 and for the local stellar surface mass density $\sigma_s(R_0)$ of 0.60 ± 0.05 kpc and $110 \pm 20\ M_\odot$ pc^{-2} respectively (van der Kruit and Shostak 1984). For the ensemble of clouds, the σ_v(c-c) obtained in § III*h* was 5.6 km s^{-1}, so that $\langle z_{1/2} \rangle_{\rm CO} =$ 191 pc. With this value, the rms scale height in the solar neighborhood is 81 pc. This value is similar to a scale height of 76 pc derived by Blitz (1978) using the midplane deviation of giant molecular cloud complexes and to a value of 55–65 pc from Cohen, Tomasevich, and Thaddeus (1979) and Sanders, Solomon, and Scoville (1984), based on data extrapolated from the inner Galaxy. All three estimates are reasonably close and so, as in Paper I, we adopt a value of 75 pc. The expectation value $\langle z \rangle$ for the height of a cloud above the midplane is thus 60 pc. In any case, the scale height of molecular matter is not expected to be greater than the H I half-thickness ($\sim$125 pc; Falgarone and Lequeux 1973). Assuming that all the clouds are at the expectation value, we obtain an expectation value for the distance to a cloud from the relation $\langle d \rangle = \langle z \rangle$ csc b. For clouds with $|b| \geq 30°$, we obtained in Paper I a mean distance $\langle \bar{d} \rangle$ for the ensemble of about 100 pc. For our high-latitude sample with $|b| \geq 25°$ we obtain $\langle \bar{d} \rangle \approx 105$ pc. This analysis indicates that the clouds as an ensemble are the nearest molecular clouds to the Sun. While individual distances may be in error, it seems highly unlikely that the statistical distance is in error by more than a factor of 2. If the distances are more than about twice our estimate, then the clouds would lie above the H I layer and, in addition, an explanation for the low velocity dispersion of the ensemble would have to be found.

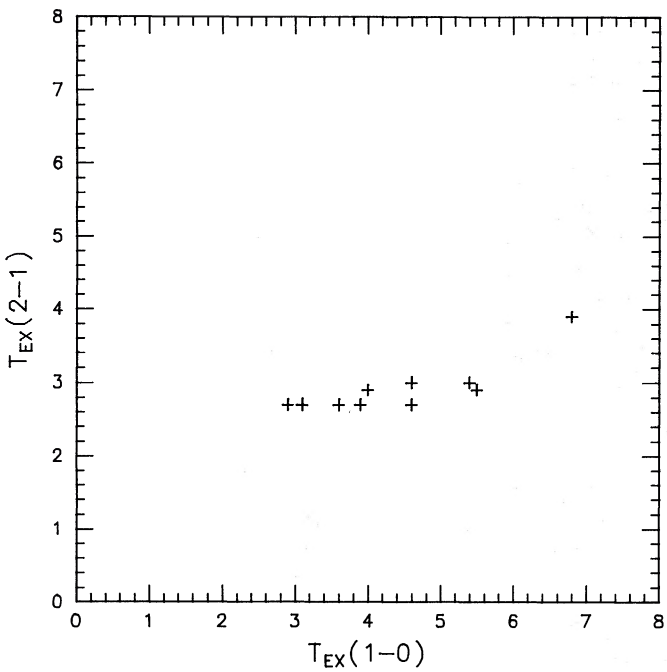

FIG. 8.—Plot of the $J = 2$–1 excitation temperature as a function of the $J = 1$–0 excitation temperature.

b) Size, Mass, and Density

Having obtained the angular size for many of the clouds, the expectation distance $\langle d \rangle$ is used to estimate the mean linear dimensions of the clouds. The mean diameter of the clouds calculated from the square root of the projected surface area is 1.7 pc; the median is 1.6 pc. The linear size of the objects is proportional to the distance, and although the sizes of individual clouds may be in error, it is unlikely that the mean size will differ substantially from these values. The clouds are quite small in spite of the large angular sizes projected by some of them.

The mass may be obtained from the column density of molecular hydrogen, $N(H_2)$, assuming that the H_2 is the main constituent of the clouds. $N(H_2)$ may be derived in two ways: from a CO/H_2 conversion factor obtained from γ-ray, CO, and H I observations of the inner Galaxy and the Orion molecular complex (Lebrun *et al.* 1983; Bloemen *et al.* 1984); and from ^{13}CO LTE assumptions (Dickman 1978). In the first case, $N(H_2) = 2.5 \times 10^{20} I_{CO}$ cm^{-2}, where I_{CO} is the integrated antenna temperature averaged over all sampled lines of sight for each complex. For the 23 complexes fully sampled, the masses determined from the column densities obtained in the manner described above range from 0.6 to 300 $M_\odot$ with a mean value of 40 $M_\odot$ and a median value of 18 $M_\odot$. An error of a factor of 2 in the distance would only change the mass by a factor of 4, so that the results of this section would not be significantly altered.

The second method for determining $N(H_2)$ requires ^{13}CO observations along the lines of sight where CO has been observed. It is assumed that the molecules along a given line of sight possess a uniform excitation temperature in the $J = 1$–0 transition, and the excitation temperatures of the CO and ^{13}CO molecules are equal. The optical depth of ^{13}CO is calculated from the excitation temperature and the $N(^{13}CO)$ is subsequently determined. Dickman's (1978) conversion factor (corrected for $A_v = 5.3 \times 10^{-22}$ $N(H_{tot})$; see § IV*c*), $N(H_2) = (4.0 \pm 2.0) \times 10^5 N(^{13}CO)$ cm^{-2}, is then used to determine $N(H_2)$. The values for the molecular column density derived in this manner are comparable to those determined from the CO/H_2 conversion factor.

If the volume is given by the projected area to the 3/2 power, the mean H_2 densities within the complexes range from 35 to 500 cm^{-3} with a mean value of 140 cm^{-3}. These values are volume-averaged densities. As the maps indicate, all the larger clouds show various degrees of clumping, so that local volume densities will be higher than the mean value. The clumped structure which exists in giant molecular clouds (e.g., Blitz 1980) appears to scale down to these smaller clouds.

c) Extinction

When the POSS prints were examined for obscuring material, no attempt was made to exclude obvious areas of high extinction such as the Lynds objects at $|b| \geq 20°$. At latitudes $|b| \geq 25°$, of the 35 complexes, five are associated with Lynds objects and thus show substantial extinction. Some complexes show no extinction and are virtually indistinguishable in appearance from many nondetections in the original search catalog. The latter cases are likely to be fluctuations in the stellar background, which become more and more widespread for $|b| > 35°$.

Using data from Bohlin, Savage, and Drake (1978), and a value for R of 3.1 (Sneden *et al.* 1978), one obtains

$$A_v = 5.3 \times 10^{-22}[N(\text{H I}) + 2N(H_2)] \text{ mag} . \tag{6}$$

In the total hydrogen column density, the contribution from H II is ignored because it is assumed to be small. Values for N(H I) are obtained from the Heiles and Habing (1974) survey. Unfortunately, it is not possible with these data to determine how much of the H I along the line of sight is associated with a given CO cloud. Upper limits for the extinction averaged over the clouds range from $A_v = 0.4$–1.6 and are listed in Table 5. Also included in the table are values for the extinction calculated for the line of sight in each cloud with the highest column density. As expected, these values show greater extinction, with a range from $A_v = 0.5$–4.8 and a median of $A_v = 1.3$. Despite the higher values in some of the cores, the high-latitude clouds are low-extinction objects with galaxies visible through several of the clouds.

d) Gravitational Binding and Age

The three-dimensional velocity dispersion of a virialized cloud given in Paper I is $\sigma_v(\text{vir}) = 0.0657(M/R)^{0.5}$ km s^{-1}, where M is the mass in solar masses and R is the equivalent radius in pc obtained in § IV*b*. For comparison with the observations, we use a one-dimensional velocity dispersion for a uniform spherical cloud $\sigma_v(\text{vir}) = 0.0293$ $(M/R)^{0.5}$ km s^{-1}. Excepting complex 30, which consists of a detection along only one line of sight, σ_v(vir) for all the mapped complexes is calculated. If the clouds are more centrally condensed with the density proportional to r^{-2}, the one-dimensional velocity dispersion increases by only a factor of 1.3, so that the conclusions of this section will not be affected. The observed internal velocity dispersion of 17 of the 22 complexes exceeds σ_v(vir) by more than a factor of 5, and 10 complexes exceed σ_v(vir) by more than an order of magnitude (see Table 5). For complexes composed of one large cloud and one or more smaller ones, using only the σ_v(int) of the large cloud does not change this result. Even an error in the distance determination could not substantially alter this result, because the dispersion for a virialized cloud depends on the distance to the 0.5 power.

To stabilize our most discrepant clouds, the distance would have to be underestimated by a factor of 200. If distance is the cause of the discrepancy between the virial velocity dispersion and the observed velocity dispersion, the molecular gas would have to be at a distance of ~ 5 kpc, which is inconsistent with the observed values of σ_v(c-c). If an anomalously high H_2/CO ratio is the cause of the above discrepancy, then the extinctions would be typically two orders of magnitude greater than those given in Table 5. However, the visibility of a number of galaxies along lines of sight which intersect the molecular clouds (e.g., IC 35 in cloud 2) rules out this possibility.

The simplest interpretation for the large observed velocity dispersions is that a large fraction of the clouds are not gravitationally bound and are breaking up. Not all our clouds are like this; some show a centrally condensed structure and $\sigma_v(\mathrm{int})/\sigma_v(\mathrm{vir})$ ratios close to 1 (i.e., cloud 45). These features are typical of quiescent clouds. As mentioned in Paper I, if the high-latitude clouds are breaking up, then their age is 10^6 yr or less. These particular clouds appear to be extraordinarily young and may represent the earliest stages of molecular material condensing from the interstellar medium (ISM).

e) Total Number and Surface Density

In Paper I the number of the detections at $|b| \geq 30°$ implied that within 100 pc of the Sun there should be $64/\epsilon$ high-latitude molecular clouds, where ϵ is the fractional incompleteness of our survey. During a subsequent run, five additional complexes were discovered, ensuring that ϵ is no greater than 0.86 and could, in fact, be much less. If $64/\epsilon$ of these objects are within 100 pc and if $\epsilon < 0.86$, then only two complexes are expected at $|b| > 80°$.

We estimate that within 150 pc of the Sun, the small molecular clouds contribute roughly $(3.0 \times 10^3)/\epsilon\ M_\odot$; this implies a mass surface density of approximately $0.1/\epsilon\ M_\odot\ \mathrm{pc}^{-2}$. For giant molecular clouds, the mean mass in the solar neighborhood is $0.5\ M_\odot\ \mathrm{pc}^{-2}$ (see Paper I). Thus, the small molecular clouds contribute an appreciable fraction of the local molecular density.

V. SUMMARY

We have presented the results of our extended survey of high Galactic latitude CO emission. A catalog of 57 distinct molecular clouds comprising 35 individual complexes at $|b| \geq 25°$ is included along with maps for 21 of the complexes. A few of the complexes were part of previously cataloged dark nebulae, but the majority represent new detections of molecular gas. The complexes are distributed all over the sky except for a stretch from $\sim 180°$ to $340°$ at northern latitudes where the H I column density also decreases. There appears to be a north-south asymmetry, with $\sim 70\%$ of the clouds south of $b = -25°$. Individual clouds subtend areas from a fraction of a square degree to several square degrees, implying that they may be responsible for at least some of the diffuse high-latitude infrared emission detected by *IRAS*.

The clouds are correlated with H I concentrations, although the molecular column density dominates in most cases. Star formation is occurring in at least one of the clouds. These star-forming sites are likely to be the nearest star-forming regions to the Sun.

The cloud-to-cloud velocity dispersion of these objects is 5.6 km s^{-1}, which implies that they are within 100 pc of the Sun. Their average sizes and masses of 1.7 pc and 40 $M_\odot$ indicate that if they are pervasive in the Milky Way, they most probably represent the small molecular cloud component of the ISM. Many of the clouds have an internal velocity dispersion which is an order of magnitude greater than the velocity dispersion obtained from the virial theorem. This, coupled with the visibility of galaxies through a number of the clouds, implies that they are not gravitationally bound. If so, their ages are 10^6 yr or less; these objects would then represent the earliest stages of molecular material condensing from the ISM. The small local clouds contribute a nonnegligible fraction of the local molecular mass surface density.

We wish to express our thanks to Bruce Wilking for assistance with the observations and for many fruitful discussions, and to Mark Morris for providing unpublished data on the Lynds 134 complex. Göran Sandell graciously provided us with his as yet unpublished identification of the T Tauri star in cloud 20. We gratefully acknowledge support from NSF grant AST 83-15276.

REFERENCES

Baran, G. P. 1982, Ph.D. thesis, Columbia University.
Belfort, P., and Crovisier, J. 1984, *Astr. Ap.*, **136**, 368.
Blaauw, A. 1960, *M.N.R.A.S.*, **121**, 164.
———. 1982, unpublished paper delivered at Leiden meeting on Southern Galactic Surveys, 1982 August.
Blitz, L. 1978, Ph.D. thesis, Columbia University.
———. 1980, in *Giant Molecular Clouds in the Galaxy*, ed. P. M. Solomon and M. G. Edmunds (Oxford: Pergamon), p. 1.
Blitz., L., Fich, M., and Stark, A. A. 1982, *Ap. J. Suppl.*, **49**, 183.
Blitz, L., Magnani, L., and Mundy, L. 1984, *Ap. J. (Letters)*, **282**, L9 (Paper I).
Blitz, L., and Thaddeus, P. 1980, *Ap. J.*, **241**, 676.
Bloemen, J. B. G. M., Caraveo, P. A., Hermsen, W., Lebrun, F., Maddalena, R. J., Strong, A. W., and Thaddeus, P. 1984, *Astr. Ap.*, **139**, 37.
Bohlin, R. C., Savage, B. D., and Drake, J. F. 1978, *Ap. J.*, **224**, 132.
Burton, W. B., and Gordon, M. A. 1978, *Astr. Ap.*, **63**, 7.
Clark, F. O., and Johnson, D. R. 1981, *Ap. J.*, **247**, 104.
Cohen, R. S., Tomasevich, G. R., and Thaddeus, P. 1979, in *IAU Symposium 84, The Large Scale Characteristics of the Galaxy*, ed. W. B. Burton (Dordrecht: Reidel), p. 53.
Dame, T. M. 1984, Ph.D. thesis, Columbia University.
de Vries, C. P., Brand, J., Israel, F. P., de Graauw, T., Wouterloot, J. G. A., van de Stadt, H., and Habing, H. J. 1984, *Astr. Ap. Suppl.*, **56**, 333.
Dickman, R. L. 1978, *Ap. J. Suppl.*, **37**, 407.
Falgarone, E., and Lequeux, J. 1973, *Astr. Ap.*, **25**, 253.
Goerigk, W., Mebold, U., Reif, K., Kalberla, P. M. W., and Velden, L. 1983, *Astr. Ap.* **120**, 63.
Goss, W. M., Manchester, R. N., Brooks, J. W., Sinclair, H. W., Manefield, G. A., and Danziger, J. J. 1980, *M.N.R.A.S.*, **191**, 533.
Heiles, C., and Habing, H. J. 1974, *Astr. Ap. Suppl.*, **14**, 1.
Israel, F. P., *et al.* 1984, *Astr. Ap.*, **134**, 396.
Kutner, M. L., and Ulich, B. L. 1981, *Ap. J.*, **250**, 341.
Lebrun, F., *et al.* 1983, *Ap. J.*, **274**, 231.
Liszt, H. S., Burton, W. B., and Xiang, D.-L. 1984, *Astr. Ap.*, **140**, 303.
Low, F. J., *et al.* 1984, *Ap. J. (Letters)*, **278**, L19.
Lynds, B. T. 1962, *Ap. J. Suppl.*, **7**, 1.
———. 1965, *Ap. J. Suppl.*, **12**, 163.
Mahoney, M. J., McCutcheon, W. H., and Shuter, W. L. H. 1976, *A.J.*, **81**, 7.
Mattila, K. 1979, *Astr. Ap.*, **78**, 253.
Mattila, K., and Sandell, G. 1979, *Astr. Ap.*, **78**, 264.
Mebold, U., and Kalberla, P. M. W. 1984, preprint.
Montani, J., Morris, M., and Thaddeus, P. 1985, in preparation.
Morris, M., Montani, J., and Thaddeus, P. 1980, in *IAU Symposium 87, Interstellar Molecules*, ed. B. H. Andrew (Dordrecht: Reidel), p. 197.
Nilson, D. N. 1973, *Uppsala General Catalogue of Galaxies* (Uppsala Obs. Ann., Vol. **6**).
Paresce, F. 1984, *A.J.*, **89**, 1022.
Paresce, F., Jakobsen, P., and Bowyer, S. 1983, *Astr. Ap.*, **124**, 300.
Penzias, A. A., and Burrus, C. A. 1973, *Ann. Rev. Astr. Ap.*, **11**, 51.

Robinson, B. J., McCutcheon, W. H., Manchester, R. N., and Whiteoak, J. B., 1983, in *Surveys of the Southern Galaxy*, ed. W. B. Burton and F. P. Israel, (Dordrecht: Reidel), p. 1.
Sandage, A. 1976, *A.J.*, **81**, 954.
Sandell, G., Johansson, L. E. B., Nguyen-Q-Rieu, and Mattila, K. 1981, *Astr. Ap.*, **97**, 317.
Sanders, D. B., Solomon, P. M., and Scoville, N. Z. 1984, *Ap. J.*, **276**, 182.
Sharpless, S. 1959, *Ap. J. Suppl.*, **4**, 257.
Sneden, C., Gehrz, R. D., Hackwell, J. A., York, D. G., and Snow, T. P. 1978, *Ap. J.*, **223**, 168.
Stark, A. A. 1979, Ph.D. thesis, Princeton University.
———. 1984, *Ap. J.*, **281**, 624.
Tucker, K. D., Dickman, R. L., Encrenaz, P. J., and Kutner, M. L. 1976, *Ap. J.*, **210**, 679.
van den Bergh, S. 1966, *A.J.*, **71**, 990.
van der Kruit, P. C. 1981, *Astr. Ap.*, **99**, 298.
van der Kruit, P. C., and Shostak, S. 1984, *Astr. Ap.*, **134**, 258.
Verschuur, G. C. 1971, *Ap. Letters*, **7**, 217.

LORIS MAGNANI and LEO BLITZ: Astronomy Program, University of Maryland, College Park, MD 20742

LEE MUNDY: Owens Valley Radio Observatory, Radio Astronomy, Robinson Laboratory, MC105-24, California Institute of Technology, Pasadena, CA 91125